articles

molecular pharmaceutics

Near-Infrared Fluorescence Labeled Anti-TAG-72 Monoclonal Antibodies for Tumor Imaging in Colorectal Cancer Xenograft Mice

Peng Zou,[†] Songbo Xu,[‡] Stephen P. Povoski,[§] Anna Wang,[†] Morgan A. Johnson,[§] Edward W. Martin, Jr.,[§] Vish Subramaniam,[||] Ronald Xu,*[,‡] and Duxin Sun*[,†]

Department of Pharmaceutical Sciences, College of Pharmacy, The University of Michigan, 428 Church Street, Ann Arbor, Michigan 48109, and Departments of Biomedical Engineering, Surgery, and Mechanical Engineering, The Ohio State University, Columbus, Ohio 43210

Received August 6, 2008; Revised Manuscript Received February 14, 2009; Accepted February 17, 2009

Abstract: Anti-TAG-72 monoclonal antibodies target the tumor-associated glycoprotein (TAG)-72 in various solid tumors. This study evaluated the use of anti-TAG-72 monoclonal antibodies, both murine CC49 and humanized CC49 (HuCC49ΔC_H2), for near-infrared fluorescent (NIR) tumor imaging in colorectal cancer xenograft models. The murine CC49 and HuCC49ΔC_H2 were conjugated with Cy7 monofunctional *N*-hydroxysuccinimide ester (Cy7-NHS). Both *in vitro* and *in vivo* anti-TAG-72 antibody binding studies were performed. The *in vitro* study utilized the human colon adenocarcinoma cell line LS174T that was incubated with Cy7, antibody−Cy7 conjugates, or excessive murine CC49 followed by the antibody−Cy7 conjugates and was imaged by fluorescence microscopy. The *in vivo* study utilized xenograft mice, bearing LS174T subcutaneous tumor implants, that received tail vein injections of Cy7, murine CC49−Cy7, HuCC49ΔC_H2−Cy7, or nonspecific IgG−Cy7 and were imaged by the Xenogen IVIS 100 system from 15 min to 288 h. The biodistribution of the fluorescence labeled antibodies was determined by imaging the dissected tissues. The *in vitro* study revealed that the antibody−Cy7 conjugates bound to LS174T cells and were blocked by excessive murine CC49. The *in vivo* study demonstrated that murine CC49 achieved a tumor/blood ratio of 15 at 96 h postinjection. In comparison, HuCC49ΔC_H2−Cy7 cleared much faster than murine CC49−Cy7 from the xenograft mice, and HuCC49ΔC_H2−Cy7 achieved a tumor/blood ratio of 12 at 18 h postinjection. In contrast, Cy7 and Cy7 labeled nonspecific IgG resulted in no demonstrable tumor accumulation. When mice were injected with excessive unlabeled murine CC49 at 6 h before the injection of murine CC49−Cy7 or HuCC49ΔC_H2−Cy7, both the intensity and retention time of the fluorescence from the tumor were reduced. In summary, the Cy7 labeled murine CC49 and HuCC49ΔC_H2 demonstrate tumor-targeting capabilities in living colorectal cancer xenograft mice and provide an alternative modality for tumor imaging.

Keywords: CC49; tumor imaging; Cy7; fluorescence; TAG-72

Introduction

Tumor associated glycoprotein 72 (TAG-72) is a human mucin (MUC1)-like glycoprotein complex, which is over-expressed in many epithelial-derived cancers, including colorectal, breast, ovarian, nonsmall cell lung, gastric, and pancreatic cancers.[1] Anti-TAG-72 monoclonal antibodies

* To whom correspondence should be addressed. Dr. Duxin Sun, Department of Pharmaceutical Sciences, College of Pharmacy, The University of Michigan, Room 2020, 428 Church Street, Ann Arbor, MI 48109. Tel: 734-615-8740. Fax: 734-615-6162. E-mail: duxins@umich.edu. Dr. Ronald Xu, Department of Biomedical Engineering, College of Engineering, The Ohio State University, Columbus, Ohio 43210.

[†] The University of Michigan.

[‡] Department of Biomedical Engineering, The Ohio State University.

[§] Department of Surgery, The Ohio State University.

[||] Department of Mechanical Engineering, The Ohio State University.

10.1021/mp9000052 CCC: $40.75
Published on Web 02/17/2009

have been studied in preclinical animal models as well as in humans for cancer detection based on their high specificity against cancer antigens in various solid cancers.[2] As previously reported, we have utilized monoclonal antibodies against TAG-72 for tumor detection in radioimmunoguided surgery (RIGS).[3−7] Historically, RIGS combined radioactive-labeled (i.e., I^{125}) monoclonal antibodies and a hand-held gamma probe for the intraoperative detection and resection of tumor-bearing tissues in colorectal cancer patients.[5] The successful detection of additional occult disease within regional lymph nodes and the subsequent complete resection of the antibody-bound tissues significantly improved survival rates.[8−11] Three generations of anti-TAG-72 antibodies (i.e., murine B72.3, murine CC49, and humanized HuCC49ΔC_H2) were evaluated by RIGS for intraoperative tumor detection and real-time guidance of surgical resection during colorectal cancer surgery.[4] B72.3 is a murine monoclonal antibody generated against TAG-72 using membrane-enriched extracts of human metastatic mammary carcinoma lesions, while murine CC49 is a second-generation murine monoclonal antibody generated against purified TAG-72 from colon cancer.[12,13] To circumvent the shortcomings of B72.3 and murine CC49, including host antimouse antibodies (HAMA) response and slow plasma clearance, a humanized CH2 domain-deleted mAb (HuCC49ΔC_H2) has been developed for RIGS.[3,4]

RIGS with anti-TAG-72 antibodies has been shown to detect 77% to 89% of primary colorectal cancers[13−15] and 78% to 97% of metastatic lesions in more than 300 patients.[3,5,8,11,14,16−23] Furthermore, RIGS detects both visible gross tumors and clinically occult disease within lymph

(1) Johnson, V. G.; Schlom, J.; Paterson, A. J.; Bennett, J.; Magnani, J. L.; Colcher, D. Analysis of a human tumor-associated glycoprotein (TAG-72) identified by monoclonal antibody B72.3. *Cancer Res.* **1986**, *46* (2), 850–857.

(2) Colcher, D.; Milenic, D.; Roselli, M.; Raubitschek, A.; Yarranton, G.; King, D.; Adair, J.; Whittle, N.; Bodmer, M.; Schlom, J. Characterization and biodistribution of recombinant and recombinant/chimeric constructs of monoclonal antibody B72.3. *Cancer Res.* **1989**, *49* (7), 1738–1745.

(3) Xiao, J.; Horst, S.; Hinkle, G.; Cao, X.; Kocak, E.; Fang, J.; Young, D.; Khazaeli, M.; Agnese, D.; Sun, D.; Martin, E. W., Jr. Pharmacokinetics and clinical evaluation of 125I-radiolabeled humanized CC49 monoclonal antibody (HuCC49deltaC(H)2) in recurrent and metastatic colorectal cancer patients. *Cancer Biother. Radiopharm.* **2005**, *20* (1), 16–26.

(4) Fang, L.; Holford, N. H. G.; Hinkle, G.; Cao, X.; Bloomston, M.; Xiao, J.; Gibbs, S.; Al Saif, O. H.; Dalton, J. T.; Chan, K. K.; Schlom, J., Jr.; Sun, D. Population Pharmacokinetics of Humanized Monoclonal Antibody HuCC49ΔCH2 and Murine Antibody CC49 in Colorectal Cancer Patients. *J. Clin. Pharmacol.* **2007**, *47*, 227–237.

(5) Nieroda, C. A.; Mojzisik, C.; Hinkle, G.; Thurston, M. O.; Martin, E. W., Jr. Radioimmunoguided surgery (RIGS) in recurrent colorectal cancer. *Cancer Detect. Prev.* **1991**, *15* (3), 225–229.

(6) Nieroda, C. A.; Mojzisik, C.; Sardi, A.; Ferrara, P.; Hinkle, G.; Thurston, M. O.; Martin, E. W., Jr. The impact of radioimmunoguided surgery (RIGS) on surgical decision-making in colorectal cancer. *Dis. Colon Rectum* **1989**, *32* (11), 927–932.

(7) Sardi, A.; Workman, M.; Mojzisik, C.; Hinkle, G.; Nieroda, C.; Martin, E. W., Jr. Intra-abdominal recurrence of colorectal cancer detected by radioimmunoguided surgery (RIGS system). *Arch. Surg.* **1989**, *124* (1), 55–59.

(8) Bertsch, D. J.; Burak, W. E., Jr.; Young, D. C.; Arnold, M. W.; Martin, E. W., Jr. Radioimmunoguided Surgery system improves survival for patients with recurrent colorectal cancer. *Surgery* **1995**, *118* (4), 634–638.

(9) Bertsch, D. J.; Burak, W. E., Jr.; Young, D. C.; Arnold, M. W.; Martin, E. W., Jr. Radioimmunoguided surgery for colorectal cancer. *Ann Surg Oncol* **1996**, *3* (3), 310–316.

(10) Gardner, B. Five-year survival after extended resection of colon cancer. *J. Surg. Oncol.* **1987**, *34* (4), 258–261.

(11) Arnold, M. W.; Young, D. C.; Hitchcock, C. L.; Schneebaum, S.; Martin, E. W., Jr. Radioimmunoguided surgery in primary colorectal carcinoma: an intraoperative prognostic tool and adjuvant to traditional staging. *Am. J. Surg* **1995**, *170* (4), 315–318.

(12) Molinolo, A.; Simpson, J. F.; Thor, A.; Schlom, J. Enhanced tumor binding using immunohistochemical analyses by second generation anti-tumor-associated glycoprotein 72 monoclonal antibodies versus monoclonal antibody B72.3 in human tissue. *Cancer Res.* **1990**, *50* (4), 1291–1298.

(13) Sickle-Santanello, B. J.; O'Dwyer, P. J.; Mojzisik, C.; Tuttle, S. E.; Hinkle, G. H.; Rousseau, M.; Schlom, J.; Colcher, D.; Thurston, M. O.; Nieroda, C. Radioimmunoguided surgery using the monoclonal antibody B72.3 in colorectal tumors. *Dis. Colon Rectum* **1987**, *30* (10), 761–764.

(14) Nieroda, C. A.; Mojzisik, C.; Sardi, A.; Ferrara, P. J.; Hinkle, G.; Thurston, M. O.; Martin, E. W., Jr. Radioimmunoguided surgery in primary colon cancer. *Cancer Detect. Prev.* **1990**, *14* (6), 651–656.

(15) Cohen, A. M.; Martin, E. W., Jr.; Lavery, I.; Daly, J.; Sardi, A.; Aitken, D.; Bland, K.; Mojzisik, C.; Hinkle, G. Radioimmunoguided surgery using iodine 125 B72.3 in patients with colorectal cancer. *Arch. Surg.* **1991**, *126* (3), 349–352.

(16) Martin, E. W., Jr.; Thurston, M. O. Intraoperative radioimmunodetection. *Semin. Surg. Oncol.* **1998**, *15* (4), 205–208.

(17) Agnese, D. M.; Abdessalam, S. F.; Burak, W. E., Jr.; Arnold, M. W.; Soble, D.; Hinkle, G. H.; Young, D.; Khazaeli, M. B.; Martin, E. W., Jr. Pilot study using a humanized CC49 monoclonal antibody (HuCC49DeltaC_H2) to localize recurrent colorectal carcinoma. *Ann. Surg. Oncol* **2004**, *11* (2), 197–202.

(18) Martinez, D. A.; Barbera-Guillem, E.; LaValle, G. J.; Martin, E. W., Jr. Radioimmunoguided Surgery for Gastrointestinal Malignancies: An Analysis of 14 Years of Clinical Experience. *Cancer Control* **1997**, *4* (6), 505–516.

(19) LaValle, G. J.; Martinez, D. A.; Sobel, D.; DeYoung, B.; Martin, E. W., Jr. Assessment of disseminated pancreatic cancer: a comparison of traditional exploratory laparotomy and radioimmunoguided surgery. *Surgery* **1997**, *122* (5), 867–871.

(20) Arnold, M. W.; Young, D. M.; Hitchcock, C. L.; Barbera-Guillem, E.; Nieroda, C.; Martin, E. W., Jr. Staging of colorectal cancer: biology vs. morphology. *Dis. Colon Rectum* **1998**, *41* (12), 1482–1487.

(21) Arnold, M. W.; Schneebaum, S.; Berens, A.; Petty, L.; Mojzisik, C.; Hinkle, G.; Martin, E. W., Jr. Intraoperative detection of colorectal cancer with radioimmunoguided surgery and CC49, a second-generation monoclonal antibody. *Ann. Surg.* **1992**, *216* (6), 627–632.

(22) Arnold, M. W.; Hitchcock, C. L.; Young, D. C.; Burak, W. E., Jr.; Bertsch, D. J.; Martin, E. W., Jr. Intra-abdominal patterns of disease dissemination in colorectal cancer identified using radioimmunoguided surgery. *Dis. Colon Rectum* **1996**, *39* (5), 509–513.

nodes in more than 70% of the cases.[11,15,16,19,22−28] These cases would be undetectable by traditional surgical and pathological examination. This occult disease (i.e., RIGS-positive tissue) within "normal" appearing lymph nodes is responsible for the development of subsequent evident-based metastatic relapse. Complete resection of this occult disease can translate into improved patient survival after surgical intervention.[29]

Despite the previous success of ^{125}I-directed RIGS in multiple previously published clinical trials, the intraoperative and postoperative handling of I^{125} as well as the disposal of I^{125} (which has a relatively long physical half-life of approximately 60 days) are the major limitations to the widespread acceptance and implementation of RIGS technology.[29] In addition, the use of ^{125}I in RIGS does not allow for the generation of high-quality preoperative imaging, which is due to the extremely low gamma photon emission energy (i.e., 35 keV) of ^{125}I, and which results in weak tissue penetration, high soft tissue attenuation, and resultant poor image quality.[30]

The near-infrared fluorescence cyanine (Cy) dyes (NIR, 650−900 nm) have been used as imaging agents for living animals due to their strong tissue penetration ability.[31−34] Various properties, such as small size, good aqueous solubility, pH insensitivity between pH 3 and 10, and low nonspecific binding, make Cy dyes good fluorescent agents for tumor imaging. Cy7 is especially suitable for the use in living animals secondary to its long excitation wavelength at 747 nm and emission wavelength at 776 nm, where autofluorescence of tissues is greatly reduced.[35] Although Cy7 is not approved for clinical use, a very similar compound (indocyanine green) has been used for human clinical applications without reported toxicity. Several intraoperative fluorescence imaging techniques have recently been described, such as endoscopic evaluation of gastrointestinal cancer[36,37] and stereomicroscopic imaging of head and neck cancer and cervical metastases, which demonstrated the potential of fluorescent immunoguided surgery.[38−41]

In this current study, we have evaluated the feasibility of using Cy7 labeled murine CC49 and HuCC49ΔC_H2 for fluorescent tumor imaging in colorectal cancer xenograft mice. We describe noninvasive fluorescent imaging of living mice and quantification of fluorescence intensities on xenograft subcutaneous tumor implants and in livers. Tumor

(23) Arnold, M. W.; Schneebaum, S.; Martin, E. W., Jr. *Cancer Control* **1996**, *3* (1), 42–45.

(24) Cote, R. J.; Houchens, D. P.; Hitchcock, C. L.; Saad, A. D.; Nines, R. G.; Greenson, J. K.; Schneebaum, S.; Arnold, M. W.; Martin, E. W., Jr. *Cancer* **1996**, *77* (4), 613–620.

(25) Sardi, A.; Agnone, C. M.; Nieroda, C. A.; Mojzisik, C.; Hinkle, G.; Ferrara, P.; Farrar, W. B.; Bolton, J.; Thurston, M. O.; Martin, E. W., Jr. Radioimmunoguided surgery in recurrent colorectal cancer: the role of carcinoembryonic antigen, computerized tomography, and physical examination. *South Med. J.* **1989**, *82* (10), 1235–1244.

(26) Kim, J. A.; Triozzi, P. L.; Martin, E. W., Jr. Radioimmunoguided surgery for colorectal cancer. *Oncology (Williston Park)* **1993**, *7* (2), 55–60.

(27) Arnold, M. W.; Schneebaum, S.; Berens, A.; Mojzisik, C.; Hinkle, G.; Martin, E. W., Jr. Radioimmunoguided surgery challenges traditional decision making in patients with primary colorectal cancer. *Surgery* **1992**, *112* (4), 624–629.

(28) Schneebaum, S.; Arnold, M. W.; Houchens, D. P.; Greenson, J. K.; Cote, R. J.; Hitchcock, C. L.; Young, D. C.; Mojzisik, C. M.; Martin, E. W., Jr. The significance of intraoperative periportal lymph node metastasis identification in patients with colorectal carcinoma. *Cancer* **1995**, *75* (12), 2809–2817.

(29) Sun, D.; Bloomston, M.; Hinkle, G.; Al-Saif, O. H.; Hall, N. C.; Povoski, S. P.; Arnold, M. W.; Martin, E. W., Jr. Radioimmunoguided surgery (RIGS), PET/CT image-guided surgery, and fluorescence image-guided surgery: Past, present, and future. *J. Surg. Oncol.* **2007**, *96* (4), 297–308.

(30) King, M. A.; Pretorius, P. H.; Farncombe, T.; Beekman, F. J. Introduction to the physics of molecular imaging with radioactive tracers in small animals. *J. Cell. Biochem.* **2002**, *39*, 221–230.

(31) Ke, S.; Wen, X.; Gurfinkel, M.; Charnsangavej, C.; Wallace, S.; Sevick-Muraca, E. M.; Li, C. Near-infrared optical imaging of epidermal growth factor receptor in breast cancer xenografts. *Cancer Res.* **2003**, *63* (22), 7870–7875.

(32) Cheng, Z.; Levi, J.; Xiong, Z.; Gheysens, O.; Keren, S.; Chen, X.; Gambhir, S. S. Near-infrared fluorescent deoxyglucose analogue for tumor optical imaging in cell culture and living mice. *Bioconjugate Chem.* **2006**, *17* (3), 662–669.

(33) Cheng, Z.; Wu, Y.; Xiong, Z.; Gambhir, S. S.; Chen, X. Near-infrared fluorescent RGD peptides for optical imaging of integrin alphavbeta3 expression in living mice. *Bioconjugate Chem.* **2005**, *16* (6), 1433–1441.

(34) Tanisaka, H.; Kizaka-Kondoh, S.; Makino, A.; Tanaka, S.; Hiraoka, M.; Kimura, S. Near-infrared fluorescent labeled peptosome for application to cancer imaging. *Bioconjugate Chem.* **2008**, *19* (1), 109–117.

(35) Hawrysz, D. J.; Sevick-Muraca, E. M. Developments toward diagnostic breast cancer imaging using near-infrared optical measurements and fluorescent contrast agents. *Neoplasia* **2000**, *2* (5), 388–417.

(36) Nimura, H.; Narimiya, N.; Mitsumori, N.; Yamazaki, Y.; Yanaga, K.; Urashima, M. Infrared ray electronic endoscopy combined with indocyanine green injection for detection of sentinel nodes of patients with gastric cancer. *Br. J. Surg.* **2004**, *91* (5), 575–579.

(37) Soltesz, E. G.; Kim, S.; Kim, S. W.; Laurence, R. G.; De Grand, A. M.; Parungo, C. P.; Cohn, L. H.; Bawendi, M. G.; Frangioni, J. V. Sentinel lymph node mapping of the gastrointestinal tract by using invisible light. *Ann. Surg. Oncol.* **2006**, *13* (3), 386–396.

(38) Gleysteen, J. P.; Newman, J. R.; Chhieng, D.; Frost, A.; Zinn, K. R.; Rosenthal, E. L. Fluorescent labeled anti-EGFR antibody for identification of regional and distant metastasis in a preclinical xenograft model. *Head Neck* **2008**, *30* (6), 782–789.

(39) Rosenthal, E. L.; Kulbersh, B. D.; King, T.; Chaudhuri, T. R.; Zinn, K. R. Use of fluorescent labeled anti-epidermal growth factor receptor antibody to image head and neck squamous cell carcinoma xenografts. *Mol. Cancer Ther.* **2007**, *6* (4), 1230–1238.

(40) Kulbersh, B. D.; Duncan, R. D.; Magnuson, J. S.; Skipper, J. B.; Zinn, K.; Rosenthal, E. L. Sensitivity and specificity of fluorescent immunoguided neoplasm detection in head and neck cancer xenografts. *Arch. Otolaryngol.* **2007**, *133* (5), 511–515.

(41) Rosenthal, E. L.; Kulbersh, B. D.; Duncan, R. D.; Zhang, W. Y.; Magnuson, J. S.; Carroll, W. R.; Zinn, K. In vivo detection of head and neck cancer orthotopic xenografts by immunofluorescence. *Laryngoscope* **2006**, *116* (9), 1636–1641.

specificity and tumor accumulation of both fluorescence labeled murine CC49 and HuCC49ΔC_H2 were observed. The images of the dissected organs showed the biodistribution and tumor-to-blood ratios of the fluorescent labeled monoclonal antibodies. In addition, the emission spectra of Cy7, murine CC49−Cy7, and HuCC49ΔC_H2−Cy7 were characterized by a noninvasive optical probe in tumors and various normal tissues/organs.

Materials and Methods

Materials. Cy7-NHS was purchased from Amersham Biosciences (Piscataway, NJ). The murine CC49 antibody was produced and purified by Rockland Immunochemicals, Inc. (Gilbertsville, PA). The HuCC49ΔC_H2 antibody was supplied by National Cancer Institute (Bethesda, MD). Phosphate buffered saline (PBS, 0.01 mol/L; pH 7.4) was purchased from Invitrogen (Carlsbad, CA). The nonspecific IgG antibodies from both human and mouse serum, as well as all other reagents, were purchased from Sigma-Aldrich Chemical Co. (St. Louis, MO).

Synthesis of Cy7 Antibody Conjugates. The pH of 1.5 mL PBS solution containing the CC49 antibody (20.5 nmol/mL) was adjusted to 8.3 by adding Na_2CO_3/$NaHCO_3$ buffer (pH = 10). A total of 1 mg of Cy7-NHS ester was dissolved in 400 μL of DMSO. 100.8 μL of Cy7-NHS ester DMSO solution (307.5 nmol) was gradually added to the CC49 solution while stirring. The solution was diluted to 2.5 mL using PBS and was stirred for 2 more hours at room temperature in the dark. The solution was loaded on a PD-10 desalting column (Amersham Biosciences, Piscataway, NJ) and washed with PBS. The murine CC49−Cy7 fraction (3.5 mL) was collected in a 10 kDa cutoff Amicon Ultra-15 centrifugal filter (Millipore Corp, Billerica, MA) and was washed with 10 mL of PBS three times (each time 5000g × 20 min). 70 nmol of HuCC49ΔC_H2, 20 nmol of murine nonspecific IgG, and 20 nmol of human nonspecific IgG were labeled with Cy7 and purified following a similar procedure. A Du640 spectrophotometer from Beckman Coulter, Inc. (Fullerton, CA) was used to determine the molar extinction coefficient of unlabeled antibodies at 280 nm (E^{280nm}) and the absorbance of the antibody−Cy7 at 280 nm (A_{280}) and 747 nm (A_{747}). The molar extinction coefficient at 747 and 280 nm of Cy7 was 200000 and 22000, respectively.[42] The ratio of the Cy7 and the antibodies of the final conjugates can be calculated with the following formula.

$$\frac{\text{Cy7}}{\text{antibody}} = \frac{[E^{280nm}A_{747}]}{[200000A_{280} - 22000A_{747}]}$$

Cell Line. Human colon adenocarcinoma cells (LS174T) were obtained from the American type Culture Collection (Manassas, VA) and cultured in Dulbecco's modified Eagle high glucose medium (DMEM) supplemented with 10% fetal bovine serum (FBS) and 1% penicillin−streptomycin (Invitrogen Life Technologies, Carlsbad, CA). The cells were maintained in a humidified atmosphere of 5% CO_2 at 37 °C, with the medium changed every other day. A confluent monolayer was detached with 0.25% trypsin-EDTA (Invitrogen Life Technologies, Carlsbad, CA) and dissociated into a single-cell suspension for further cell culture.

***In Vitro* Binding Studies.** Cells were cultured on 4-well chamber slides (Thermo Fisher Scientific, Rochester, NY) and incubated in a humidified atmosphere of 5% CO_2 at 37 °C overnight. After washing twice with PBS, the cells were incubated in 3.7% paraformaldehyde for 15 min and then washed again with PBS. Cy7 (0.5 nmol), murine CC49−Cy7 (0.49 nmol equivalent Cy7) or HuCC49ΔC_H2−Cy7 conjugate (0.49 nmol equivalent Cy7) was added into each well and diluted to 0.3 mL with PBS. For the blocking study, murine CC49 antibody (4 nmol) was added 1 h before the addition of murine CC49−Cy7 or HuCC49ΔC_H2 −Cy7 conjugate. After an incubation period of 2 h at room temperature, cells were washed with PBS (5 min × 4). The coverslips were mounted with a drop of fluoromount G (Southern Biotech, Birmingham, AL). Microscopic examination was conducted on a Zeiss-Axiophot microscope (Carl Zeiss, Inc., Jena, German). The microscope is equipped with a RT KE slider digital camera (Diagnostic Instruments Inc. Sterling Heights, MI), a HBO 103 W/2 mercury lamp (Carl Zeiss, Inc., Jena, German), a Cy7 filter set with an excitation wavelength of 680−740 nm and an emission wavelength of 775−850 nm (Chroma Technology Corp., Rochingham, VT), and a Metavue software (Molecular Devices, Downingtown, PA) for image acquisition, processing, and analysis. The image magnification is 100×. The exposure time is 4000 ms for the fluoresence images and 300 ms for the transparent images. The space resolution for all images is 1600 × 1200 pixels, and image bit depth is 24 bit. The pseudocolor of Cy7 is red.

Tumor Xenografts. The animal procedures were performed according to a protocol approved by the by the University Committee for the Use and Care of Animals (UCUCA) at The Ohio State University. Female athymic nude mice (nu/nu), obtained from National Cancer Institute (Bethesda, MD) at 4 to 6 weeks of age, were subcutaneously inoculated in the back with 5×10^6 LS174T cells suspended in a mixture of 50 μL of PBS and 50 μL of matrixgel basement membrane (BD Biosciences, San Jose, CA). When the tumor implants reached 0.4 to 0.6 cm in diameter (approximately 14 days after implantation), the tumor-bearing mice were subjected to the *in vivo* studies.

***In Vivo* Optical Tumor Imaging.** *In vivo* fluorescence imaging was performed with an IVIS 100 small animal imaging system (Xenogen, Alameda, CA). An ICG filter (excitation wavelength 710−760 nm and emission wavelength 810−875 nm) was used for acquiring Cy7, murine CC49−Cy7, HuCC49ΔC_H2−Cy7, and nonspecific IgG−Cy7 fluorescence imaging *in vivo*. Identical illumination settings, such as exposure time (1 s), binning factor (8), *f*/stop (1), and fields of view (25 × 25 cm), were used for acquiring all images, and fluorescence emission was normalized to

(42) Healthcare, G. Protocol for Amersham CyDye monoreactive NHS Esters. 2006.

photons per second per centimeter squared per steradian ($p\ s^{-1}\ cm^{-2}\ sr^{-1}$). The imaging was acquired and overlaid. The pseudocolor image represents the spatial distribution of photon counts within the animal. Background fluorescence was measured and subtracted by setting up a background measurement. Images were acquired and analyzed using Living Image 2.5 software (Xenogen, Alameda, CA).

Mice bearing LS174T tumor were injected via the tail vein with 1 nmol of Cy7-NHS, 0.33 nmol of murine CC49−Cy7 (1 nmol equivalent Cy7/mouse), 0.73 nmol of HuCC49ΔC_H2−Cy7 (1 nmol equivalent Cy7/mouse), 0.38 nmol of nonspecific murine IgG−Cy7, or 0.50 nmol of nonspecific human IgG−Cy7 (1 nmol equivalent Cy7/mouse). For the blocking study, 3.3 nmol of unlabeled murine CC49 was injected (iv) 6 h before injection of the conjugates. One mouse bearing the LS174T tumor was not injected and was used as a blank control. Mice were anesthetized with isoflurane (Abbott Laboratories, Chicago, IL), and images were obtained every 15 min for up to 3 h after injection of each fluorescent antibody. Each mouse was imaged again 4, 5, 6, 7, 18, 24, 48, 72, 96, and 288 h after injection of each fluorescent antibody. Both the dorsal and ventral sides of each mouse were imaged. The tumor area and the liver area were designated as the two regions of interest (ROI). The relative mean fluorescent intensity of each ROI was obtained by subtracting the mean fluorescence intensity of the corresponding ROI on the blank mouse from the measured mean fluorescent intensity and was plotted as a function of time.

Optical Imaging of Fresh Tissues. As described above in *in vivo* tumor imaging, two additional groups of LS174T tumor xenograft mice were given Cy7-NHS, murine CC49−Cy7, murine CC49/murine CC49−Cy7, or nonspecific murine IgG−Cy7. One group of mice was sacrificed at 2 h and the other group of mice was sacrificed at 96 h after intravenous injection of fluorescent marker tagged antibodies. Following the same procedure, two additional groups of LS174T tumor xenograft mice were given Cy7-NHS, HuCC49ΔC_H2−Cy7, murine CC49/HuCC49ΔC_H2−Cy7 or nonspecific human IgG−Cy7 and sacrificed at 2 and 18 h postinjection, respectively. The dissected tissues (tumor, spleen, kidneys, lung, heart, liver, stomach, and intestine) were imaged immediately. The mean fluorescent intensity of each tissue sample was obtained by subtracting the mean fluorescent intensity of corresponding tissue from the blank mouse. The fluorescent intensities in the heart were used to reflect the fluorescent intensities in the blood. The tissue to heart ratio for fluorescence was calculated.

Noninvasive Measurement of Fluorescent Emission Spectra. All the fluorescent emission spectra were measured using a USB4000-FL fluorescence spectrometer (Ocean Optics Inc., Dunedin, FL). A HL6738MG diode laser (Thorlabs, Newton, NJ) was used to excite the samples at the wavelength of 690 nm. To measure the emission spectra of contrast agents in cuvettes, the excitation laser beam was incident from one side of the cuvette. The detector and a 715 nm long pass filter (Thorlabs, Newton, NJ) were placed in a direction perpendicular to the excitation laser beam. For the measurement of emission spectra from organs in living animals, the excitation laser source was oriented perpendicular to the animal skin above the specific organs. The detector and the 715 nm long pass filter were aligned at 45 degree to the laser beam. The measurement was carried out 24 h postinjection of murine CC49−Cy7. The raw data was processed by the Matlab curve fitting toolbox (The Mathworks Inc., Natick, MA). Local regression with weighted linear least-squares and a first degree polynomial model were used for curve fitting the spectrum.

Results

Synthesis of Murine CC49−Cy7 and HuCC49ΔC_H2−Cy7. The antibody was labeled with Cy7-NHS ester by acylating the primary amines of the antibody. The 280 nm emission line, E^{280nm} of murine CC49 and HuCC49ΔC_H2 were measured to be 157000 $M^{-1}\ cm^{-1}$ and 182400 $M^{-1}\ cm^{-1}$ respectively. The Cy7/murine CC49 ratio, Cy7/HuCC49ΔC_H2 ratio, Cy7/murine IgG ratio, and Cy7/human IgG ratio were determined to be 3.02, 1.36, 2.60, and 2.01, respectively.

***In Vitro* Binding Studies.** Figure 1 shows the fluorescent microscopic images of LS174T cells incubated with PBS, Cy7, murine CC49−Cy7 conjugate, murine CC49 plus murine CC49−Cy7 conjugate, HuCC49ΔC_H2−Cy7 conjugate, and murine CC49 plus HuCC49ΔC_H2−Cy7 conjugate. No autofluorescence was detected from the cells incubated with PBS, and negligible signals were detected from cells incubated with Cy7. In contrast, fluorescent signals were observed from cells incubated with murine CC49−Cy7 or HuCC49ΔC_H2−Cy7 conjugate, suggesting that both conjugates bound to the cells. Furthermore, binding of murine CC49−Cy7 or HuCC49ΔC_H2−Cy7 to the cells was completely blocked when the cells were pretreated with excessive murine CC49 antibody.

***In Vivo* Optical Tumor Imaging.** As previously reported, the LS174T tumor has a high level of TAG-72 expression.[43] Whole-body imaging of subcutaneous LS174T tumor xenograft mice was accomplished by using an IVIS 100 system to monitor *in vivo* biodistribution of murine CC49−Cy7 and HuCC49ΔC_H2−Cy7. Figure 2A shows typical NIR images of mice bearing LS174T tumors 15 min and 96 h after iv injection of Cy7 or murine CC49−Cy7. No autofluorescence was detected from the blank mouse. The fluorescent signal was detected from the whole body of a mouse 15 min after injection of Cy7, suggesting the rapid distribution of Cy7 in the mouse body. Subsequently, Cy7 is rapidly eliminated from the kidney, and no fluorescence was detected on this mouse 96 h postinjection. In contrast, a fluorescent signal

(43) Fang, L.; Battisti, R. F.; Cheng, H.; Reigan, P.; Xin, Y.; Shen, J.; Ross, D.; Chan, K. K.; Martin, E. W., Jr.; Wang, P. G.; Sun, D. Enzyme specific activation of benzoquinone ansamycin prodrugs using HuCC49DeltaCH2-beta-galactosidase conjugates. *J. Med. Chem.* **2006**, *49* (21), 6290–6297.

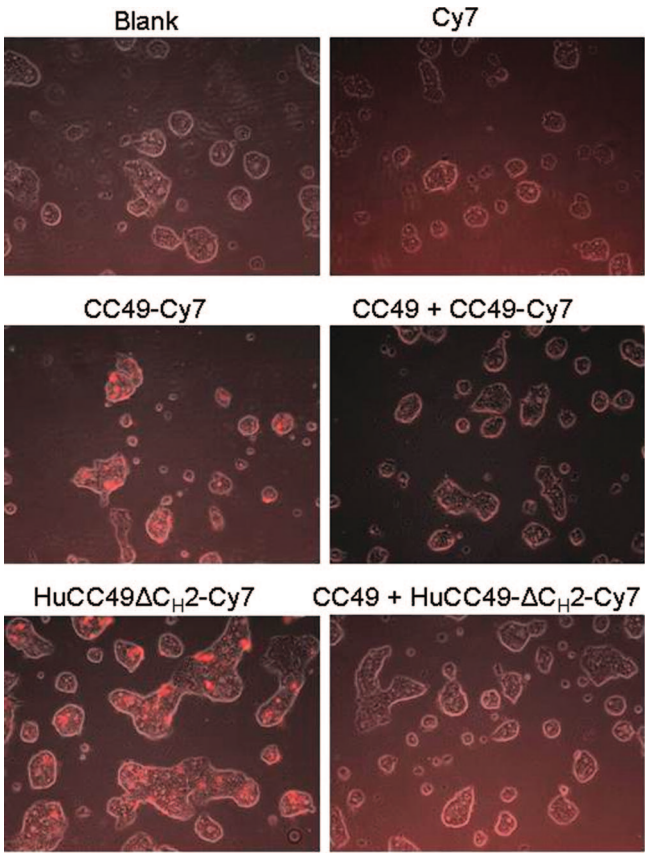

Figure 1. Fluorescence microscopic images of LS174T cells. The cells were fixed with 3.7% paraformaldehyde and incubated for 1 h at room temperature with PBS, Cy7, murine CC49−Cy7, murine CC49 followed by murine CC49−Cy7, HuCC49ΔC$_H$2−Cy7, and murine CC49 followed by HuCC49ΔC$_H$2−Cy7.

was detected from the abdominal area of the mice injected with the murine CC49−Cy7 or murine IgG−Cy7, suggesting the distribution of the antibody−Cy7 in the liver or spleen immediately postinjection. 96 h postinjection, fluorescence of murine CC49−Cy7 was clearly visualized in the tumors of two mice while the fluorescence of nonspecific murine IgG−Cy7 was hard to be detected. The previously observed fluorescence from the abdominal area did not present. When the mice were injected with the unlabeled murine CC49 before administration of the murine CC49−Cy7 (i.e., blocked), the fluorescent intensity from the tumor was found to be significantly lower than that from the tumor of the murine CC49−Cy7 mouse. This suggests that the TAG-72 was blocked by excessive murine CC49 antibody.

Similar results were obtained when HuCC49ΔC$_H$2−Cy7 was used as the imaging agent (Figure 2B). The tumor could clearly be visualized from the surrounding background tissues 18 h postinjection of HuCC49ΔC$_H$2−Cy7 while no fluorescence signal was detected from the tumor of the mouse blocked with excessive murine CC49 antibody and the mouse injected with nonspecific human IgG−Cy7. Intense fluorescence signal was still detected from the abdominal areas of the mouse injected with HuCC49ΔC$_H$2−Cy7 and the blocked mouse 18 h after injection of HuCC49ΔC$_H$2−Cy7. This data suggests that both HuCC49ΔC$_H$2−Cy7 and murine CC49−Cy7 are able to target tumors for noninvasive fluorescent tumor imaging. Nevertheless, HuCC49ΔC$_H$2−Cy7 may have faster clearance than murine CC49−Cy7 in xenograft models.

Noninvasive Characterization of Emission Spectra of Fluorescent Agents from Tissues. The emission spectra from Cy7 and murine CC49−Cy7 solutions as well as from the tissues in the living mice were recorded with a USB4000-FL fluorescence spectrometer. As shown in Figure 3, the maximum emission wavelengths of Cy7 and murine CC49−Cy7 solution were determined to be 770.3 and 777.1 nm, respectively. A shift in the maximum emission of 6.9 nm to longer wavelengths was detected when Cy7 was attached to the murine CC49 antibody. The maximum emission wavelengths of fluorescent signals from the liver, tumor and bladder of the mouse injected with murine CC49−Cy7 were determined to be 778.5 nm, 778.9 nm and 776.1 nm, respectively.

Dynamic Fluorescence Intensities in Tumors and Livers. The fluorescent intensities from the tumors and livers were measured noninvasively during a period of 0 to 288 h after the injection of Cy7, murine CC49−Cy7, or HuCC49ΔC$_H$2−Cy7. The measured intensities were then reduced to relative values by subtracting the mean fluorescence intensity from the tumor or liver of the blank mouse. Figure 4 shows the relative fluorescence intensity as a function of time for the regions of interest corresponding to tumors and livers. Both the maximum intensities (C_{max}) and retention times (T_{max}) of fluorescence from the tumor are different among Cy7, blocked, and murine CC49−Cy7 mice (Figure 4A). The concentration of Cy7 in the tumor decreased rapidly, and Cy7 was completely eliminated from the tumor 4 h postinjection. The tumor fluorescence in the mouse injected with the murine CC49−Cy7 reached the highest intensity at 48 h postinjection and remained so between 72 and 120 h. Tumor fluorescence was detected as far as 288 h postinjection. In contrast, the peak fluorescent intensity from the tumor of the mouse with excessive unlabeled murine CC49 was detected at 24 h postinjection, after which the intensity decreased rapidly. The fluorescent intensity from the tumor of the mouse with excessive unlabeled murine CC49 was significantly lower than that from the tumor of the murine CC49−Cy7 mouse. Figure 4C shows the dynamic biodistribution of HuCC49ΔC$_H$2−Cy7 in the tumors. The mouse with HuCC49ΔC$_H$2−Cy7 as well as the mouse with excessive unlabeled murine CC49 and HuCC49ΔC$_H$2−Cy7 showed the highest fluorescent intensities from the tumors 5 h after injection of HuCC49ΔC$_H$2−Cy7. The elimination of HuCC49ΔC$_H$2−Cy7 from the tumors was much faster than the removal of murine CC49−Cy7. When the mouse was pretreated with excessive murine CC49, the fluorescent intensity from the tumor was significantly lower than that in the tumor of the unblocked HuCC49ΔC$_H$2−Cy7 mouse. The murine CC49 blockage also decreased the retention time of HuCC49ΔC$_H$2−Cy7 in the tumor from 96 to 48 h. This data suggests that the HuCC49ΔC$_H$2−Cy7 and murine CC49−Cy7 target LS174T tumors antigen-specifically.

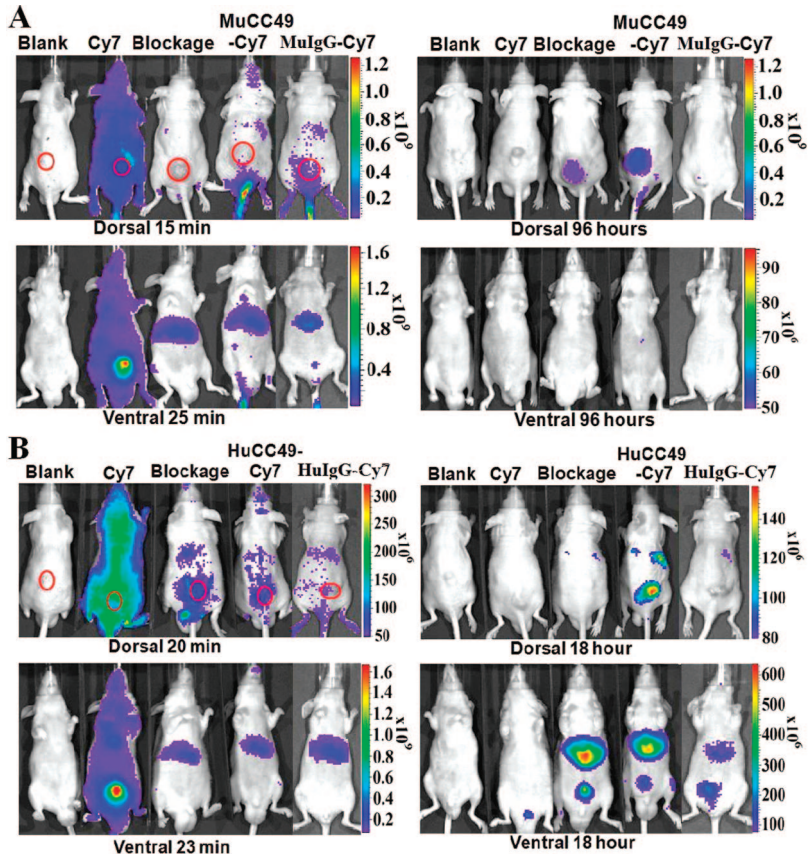

Figure 2. Typical *in vivo* fluorescence images of athymic nude mice bearing LS174T xenografts after intravenous injection of (A) 1 nmol of Cy7, excessive murine CC49 followed by 0.33 nmol of murine CC49−Cy7, 0.33 nmol of murine CC49−Cy7, or 0.38 nmol of nonspecific murine IgG−Cy7; (B) 1 nmol of Cy7, excessive murine CC49 followed by 0.73 nmol of HuCC49ΔC_H2−Cy7, 0.73 nmol of HuCC49ΔC_H2−Cy7, or 0.50 nmol of nonspecific human IgG−Cy7. The location of the tumors is indicated by the circles.

In contrast, murine CC49−Cy7 and HuCC49ΔC_H2−Cy7 exhibit maximum concentrations in the liver at 6 h postinjection for both murine CC49−Cy7 and HuCC49ΔC_H2−Cy7 mice, as well as the mice pretreated with excessive murine CC49 (Figure 4B, D). No obvious difference in fluorescent intensity from the liver was found between the two groups of mice. Fluorescence from the livers of both mice disappeared 96 h after the injection of murine CC47−Cy7 and HuCC49ΔC_H2−Cy7. This data suggests that the accumulation of murine CC47−Cy7 and HuCC49 ΔC_H2−Cy7 in the liver is nonspecific.

Analysis of Fluorescence from Fresh Tissues. Fluorescent signals from different freshly dissected tissues were quantified by optical imaging. Figure 5A shows the images of dissected tissues of blank, Cy7, murine CC49 pretreated, murine CC49−Cy7, and nonspecific murine IgG−Cy7 mice that were sacrificed at 2 or 96 h postinjection of fluorescent agents. Figure 6A shows the images of dissected tissues of blank, Cy7, murine CC49 pretreated, HuCC49ΔC_H2−Cy7, and nonspecific human IgG−Cy7 mice that were sacrificed at 2 or 18 h postinjection of fluorescent agents. The relative fluorescent intensity from each tissue, obtained by subtracting the mean fluorescent intensity from the corresponding tissue of the blank mouse, is labeled in Figures 5A and 6A. The tissue imaging data revealed that the fluorescent signals from the abdomen and pelvis of the mice were mainly due to the distribution of antibody−Cy7 in the liver, gastrointestinal tract, spleen, and kidneys. A low level of autofluorescence was detected from the stomach and intestines even though no fluorescent agent was injected to the blank mouse. As shown in Figures 5A and 6A, Cy7 was mainly distributed in kidneys, tumor, and stomach 2 h postinjection. A small amount of fluorescence was detected from the spleen and liver. Cy7 was completely eliminated from all tissues at 18 h postinjection. In the murine CC49−Cy7 mice, murine CC49−Cy7 was mainly distributed in the liver, lung, kidneys, spleen, heart and tumor at 2 h postinjection (Figure 5A). Most fluorescence from the spleen, kidneys, lung, and heart appeared to be cleared at 96 h postinjection. The fluorescence intensities from the tumors doubled while the fluorescence intensities from the livers decreased. The fluorescence intensity from the tumor of the murine CC49−Cy7 mouse was higher than that from the tumor of the mouse pretreated with excessive murine CC49. The nonspecific murine IgG−Cy7 mainly localized in liver and kidneys 2 h postinjection and was cleared from the body 96 h postinjection. The fluorescent intensity from the heart was used to reflect the fluorescent intensity from the blood. Figures 5B and 5C show the tissue to heart ratios for the fluorescence at 2 and 96 h after injection of Cy7, murine CC49−Cy7, or

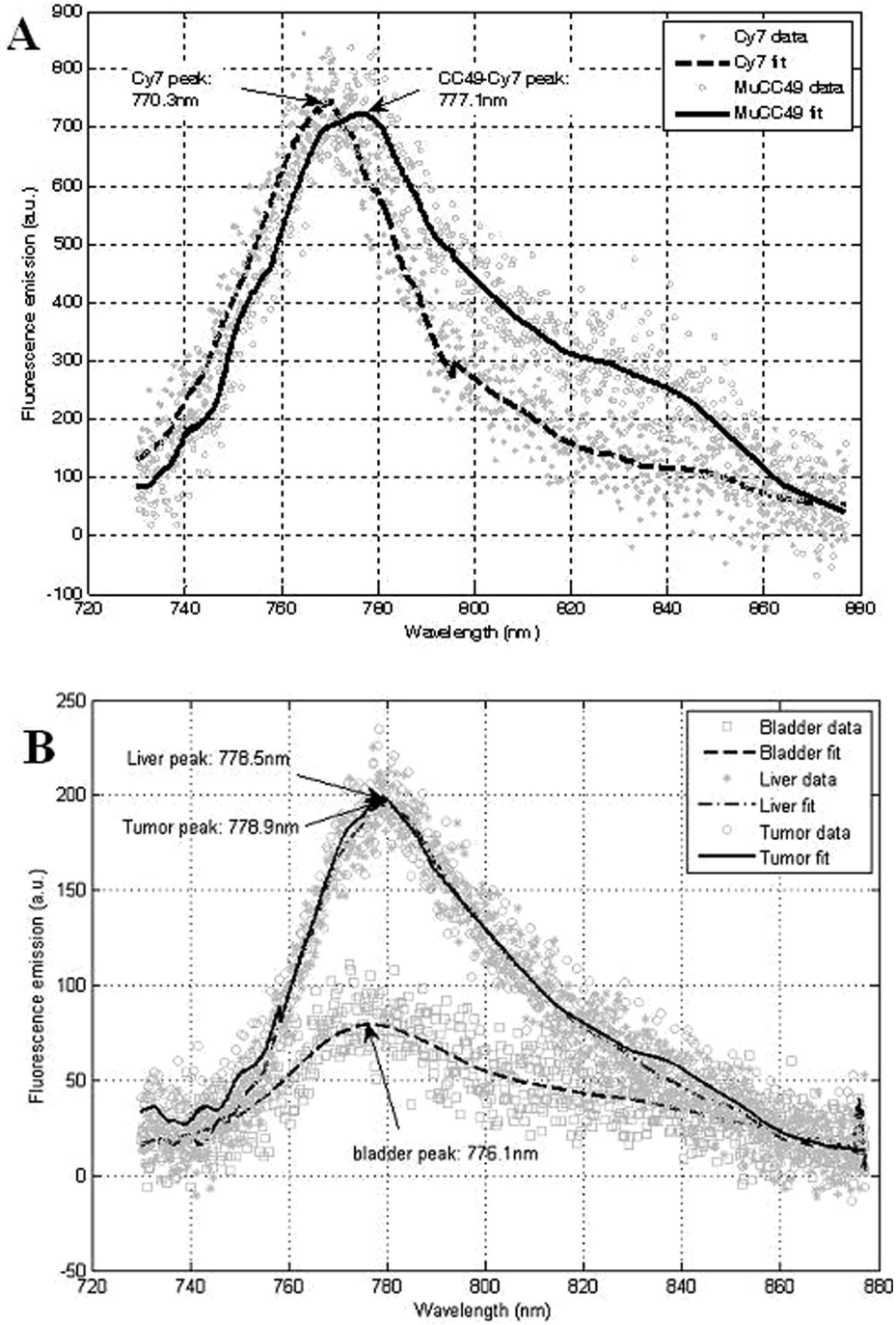

Figure 3. Emission spectra of (A) Cy7 and murine CC49−Cy7 and (B) fluorescence signals from the bladder, liver and tumor of an athymic nude mouse bearing LS174T xenograft tumor 24 h after iv injection of murine CC49−Cy7.

nonspecific murine IgG−Cy7. From 2 to 96 h postinjection, the tumor to heart ratio for the murine CC49−Cy7 mouse increased from 1.3 to 15.5 and the tumor to heart ratio for the mouse pretreated with excessive murine CC49 increased from 0.7 to 9.9. In contrast, the tumor to heart ratio for the Cy7 mouse decreased from 2.9 to 1.3 while the tumor to heart ratio for the nonspecific murine IgG−Cy7 mouse slightly increased from 0.65 to 1.62. In the murine CC49−Cy7 mouse as well as the mouse pretreated with excessive murine CC49, the spleen to heart, kidneys to heart, and lung to heart ratios decreased or remained unchanged while the liver to heart ratios increased.

Much like murine CC49−Cy7, HuCC49ΔC_H2−Cy7 was mainly distributed in the tumor, liver, spleen, kidneys, lung, and heart. The fluorescent signal detected from the stomach and intestine of the mice may be due to autofluorescence. Figures 6B and 6C show the tissue to heart ratios for the fluorescence at 2 and 18 h after injection of Cy7, HuCC49ΔC_H2−Cy7 or nonspecific human IgG−Cy7. From 2 to 18 h postinjection, only the tumor and the liver had a

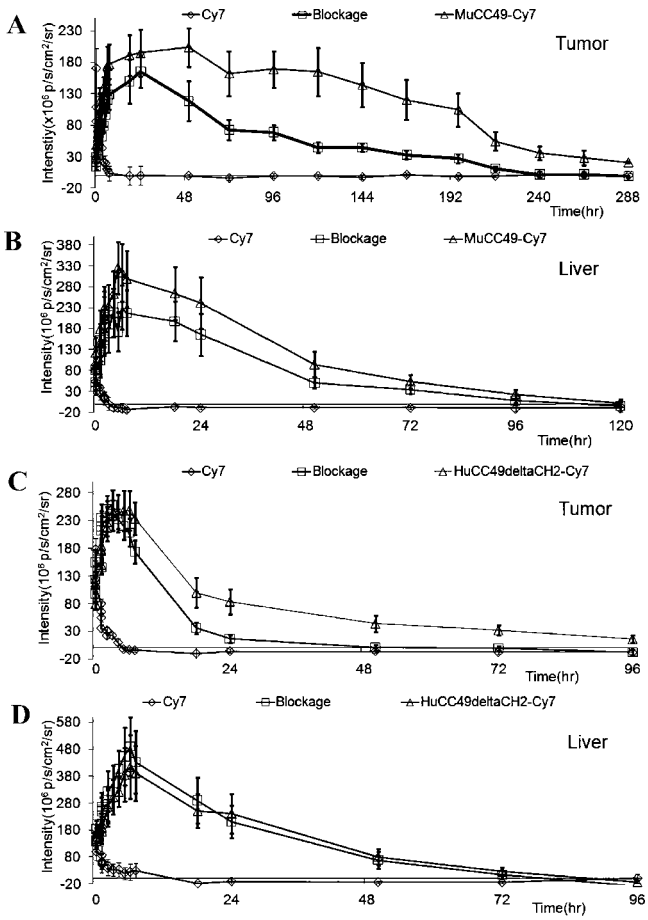

Figure 4. The relative mean fluorescence intensity in the tumor and liver regions of interest (ROIs) as a function of time after injection of (A, B) Cy7, excessive murine CC49 plus murine CC49−Cy7, or murine CC49−Cy7 and (C, D) Cy7, excessive murine CC49 plus HuCC49ΔC_H2−Cy7, or HuCC49ΔC_H2−Cy7.

dramatic increase of fluorescent intensity. The tumor to heart ratio for the HuCC49ΔC_H2−Cy7 mouse increased from 2.1 to 12.0 and the tumor to heart ratio for the mouse pretreated with excessive murine CC49 increased from 0.9 to 9.8. In contrast, the tumor to heart ratio for the Cy7 mouse decreased from 3.4 to 0.2 and the tumor to heart ratio for the nonspecific human IgG−Cy7 mouse decreased from 1.94 to 1.47. For the murine CC49−Cy7 mice, the spleen to heart, kidneys to heart and lung to heart ratios decreased or showed no change while the liver to heart ratios increased.

Discussion

NIR fluorescence imaging is emerging as a powerful tool for noninvasive imaging for use in both preclinical and clinical investigations. In this regard, it has great potential for use in the arena of clinical cancer diagnosis and for monitoring of cancer therapeutics.[44] Our previous studies[11−19] have shown that human cancer cell lines LS174T and human colorectal cancer tissues express high levels of TAG-72. Radioisotope-labeled murine CC49 and HuCC49ΔC_H2 antibodies localize and target more than 80% of colorectal cancer in both preclinical testing and clinical investigations. Encouraged by these results, we hypothesize that conjugation of the murine CC49 and HuCC49ΔC_H2 antibodies with Cy7 will not change the cancer targeting ability of the antibody and that the conjugates can be used for tumor imaging in living subjects. Therefore, the murine CC49−Cy7 and HuCC49ΔC_H2−Cy7 conjugates were synthesized and evaluated in a colorectal cancer xenograft mice model.

When labeling antibodies with NHS esters, it is necessary to optimize the ratio of NHS ester to antibody and pH in order to give the final Cy dye to protein (D/P) ratio that yields maximum fluorescence. A previous study on Cy5 found that the brightest antibodies had a D/P ratio of 2−3.[45] However, no fluorescence was observed for a D/P ratio of 6 secondary to the self-quenching characteristics of the fluorescent dye. Another study conducted by GE Healthcare showed that Cy NHS ester to antibody ratios of 1:1, 5:1, 10:1, and 20:1 gave final D/P ratios of 0.28:1, 1.16:1, 2.3:1, and 4.6:1, respectively.[29] Considering all the above factors, we selected a ratio of Cy7 NHS ester to antibody of 10:1 in the synthesis reaction. In addition, the pH is also known to affect the D/P ratio. D/P ratios of 5−6 were obtained after ten minutes using a pH 8.5 to 9.4.[46] To obtain D/P of 2−3, we used a pH of 8.3. The final Cy7/murine CC49 ratio was 3.02, and the final Cy7/ HuCC49ΔC_H2 ratio was only 1.36. The low labeling efficiency of HuCC49ΔC_H2 can be explained due to the fact that the HuCC49ΔC_H2 was chelated by DOTA, which consumed some primary amino groups on the antibody.

Cy5.5 is a widely used cyanine dye for NIR fluorescence imaging of living animals.[31] However, Cy5.5 may have low tissue penetration and autofluorescence from imaging larger tissue volumes.[35] Ke et al.[31] reported that the contents in the gastrointestinal tract from the mouse's diet might cause intense autofluorescence and reduce the imaging efficacy of Cy5.5 labeled target protein. In our whole-body imaging with antibody−Cy7, no autofluorescence was detected from the abdominal and pelvic areas of the blank mice (Figure 2). Only limited autofluorescence was found in the images of the dissected stomach and intestines of the blank mouse (Figures 5 and 6), which might have resulted from the diet. Compared with Cy5.5, the longer excitation and emission wavelengths of Cy7 provides increased tissue penetration with minimal tissue autofluorescence.[35]

The *in vitro* binding studies (Figure 1) showed the specific binding between the antibody−Cy7 conjugate and the LS174T cells. The possibility of nonspecific binding between

(44) Xu, R. X.; Povoski, S. P. Diffuse optical imaging and spectroscopy for cancer. *Expert Rev. Med. Devices* **2007**, *4* (1), 83–95.

(45) Gruber, H. J.; Hahn, C. D.; Kada, G.; Riener, C. K.; Harms, G. S.; Ahrer, W.; Dax, T. G.; Knaus, H. G. Anomalous fluorescence enhancement of Cy3 and Cy3.5 versus anomalous fluorescence loss of Cy5 and Cy7 upon covalent linking to IgG and noncovalent binding to avidin. *Bioconjugate Chem.* **2000**, *11* (5), 696–704.

(46) Mujumdar, R. B.; Ernst, L. A.; Mujumdar, S. R.; Lewis, C. J.; Waggoner, A. S. Cyanine dye labeling reagents: sulfoindocyanine succinimidyl esters. *Bioconjugate Chem.* **1993**, *4* (2), 105–111.

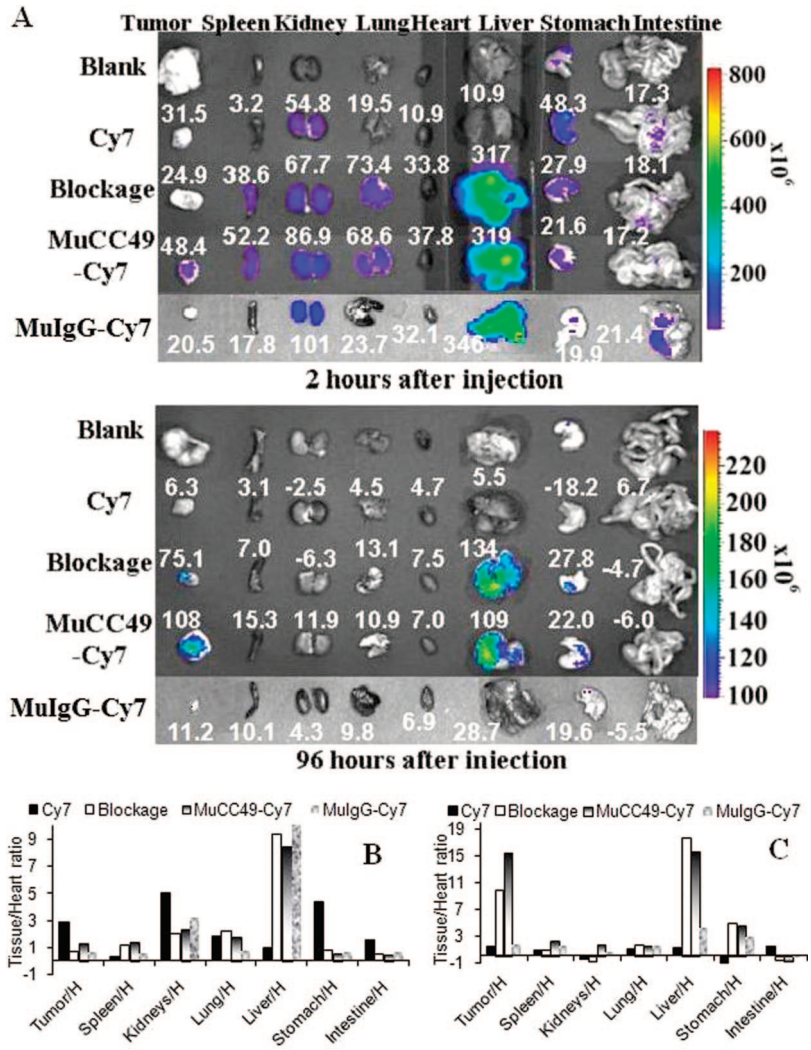

Figure 5. (A) Representative images of dissected organs of athymic nude mice bearing LS174T xenograft tumor sacrificed 2 or 96 h after intravenous injection of 1 nmol of Cy7, excessive murine CC49 followed by 0.33 nmol of murine CC49−Cy7, 0.33 nmol of murine CC49−Cy7, or 0.38 nmol nonspecific murine IgG−Cy7. The relative fluorescence intensity of each tissue was labeled near the corresponding tissue. Tissue-to-heart ratios for (B) the mice sacrificed 2 h after injection and (C) the mice sacrificed 96 h after injection.

free Cy7 and LS174T cells was excluded by the finding that negligible fluorescence was detected from the cells incubated with free Cy7. Furthermore, excessive CC49 antibody successfully blocked the binding of murine CC49−Cy7 or HuCC49ΔC_H2−Cy7 to the LS174T cells, indicating that the binding was mediated through TAG-72.

The dynamic imaging data revealed different pharmacokinetics and distribution of Cy7, murine CC49−Cy7, and HuCC49ΔC_H2−Cy7. The rapid distribution and elimination of Cy7 in the whole mouse body can be explained by its very small molecular weight (818 Da). In contrast, only a limited amount of fluorescence was detected 15 min after injection of the antibody−Cy7 conjugate, suggesting that its larger molecular size of may be responsible in slowing down its diffusion and distribution. The dynamic imaging data also illustrated that the HuCC49ΔC_H2−Cy7 conjugate was cleared from the body of the mouse much faster than the murine CC49−Cy7 conjugate, which is consistent with the previously reported data. Previous studies with ^{125}I- or ^{177}Lu-labeled murine CC49 in non-tumor-bearing athymic mice gave $t_{1/2\alpha}$ values ranging from 1.8 to 5.6 h and $t_{1/2\beta}$ values in the range of 77.2 to 179.4 h.[47] Studies with ^{177}Lu-labeled HuCC49ΔC_H2 administered intravenously to LS174T tumor-bearing athymic mice yielded a $t_{1/2\alpha}$ of 13.3 min and a $t_{1/2\beta}$ of 5.3 h.[48] Another study showed a shorter plasma clearance $t_{1/2}$ of ^{177}Lu-labeled HuCC49ΔC_H2 at 2.7 h.[49] The faster clearance of HuCC49ΔC_H2 is due to the C_H2 domain deletion, which prevents the binding between HuCC49ΔC_H2 and FcRn receptors. The unbound HuCC49ΔC_H2 undergoes lysosomal degradation and cannot recycle into serum.[47]

Murine CC49−Cy7 conjugate demonstrated a longer retention time in the tumor (288 h) compared to the

(47) Slavin-Chiorini, D. C.; Kashmiri, S. V.; Schlom, J.; Calvo, B.; Shu, L. M.; Schott, M. E.; Milenic, D. E.; Snoy, P.; Carrasquillo, J.; Anderson, K. Biological properties of chimeric domain-deleted anticarcinoma immunoglobulins. *Cancer Res.* **1995**, *55* (23), 5957s–5967s.

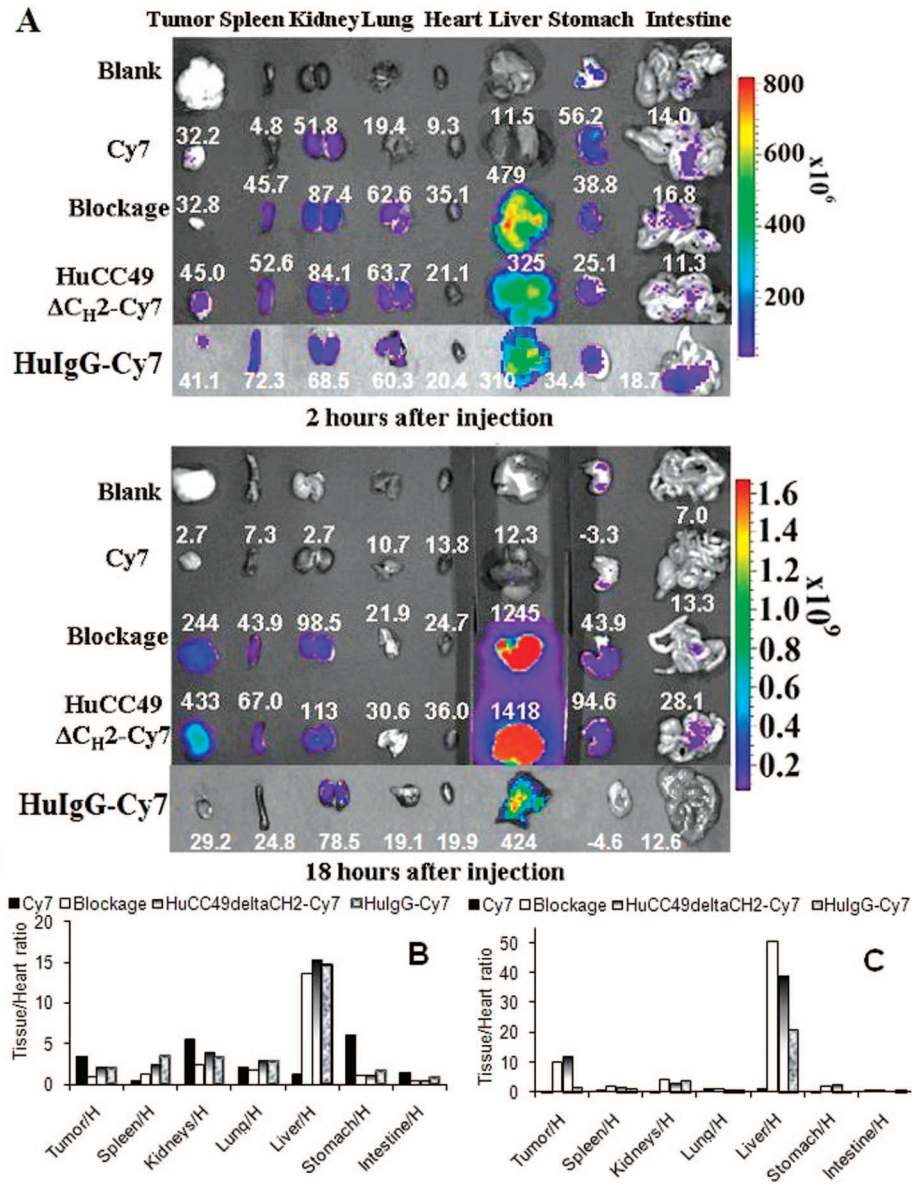

Figure 6. (A) Representative images of dissected organs of athymic nude mice bearing LS174T xenograft tumor sacrificed 2 or 96 h after intravenous injection of 1 nmol of Cy7, excessive murine CC49 followed by 0.73 nmol HuCC49ΔC_H2−Cy7, 0.73 nmol HuCC49ΔC_H2−Cy7, or 0.50 nmol nonspecific human IgG−Cy7. The relative fluorescence intensity of each tissue was labeled near the corresponding tissue. Tissue-to-heart ratios for (B) the mice sacrificed 2 h after injection and (C) the mice sacrificed 18 h after injection.

HuCC49ΔC_H2−Cy7 conjugate (96 h), likely due to the long plasma clearance half-life of the murine CC49−Cy7 conjugate. The slow plasma clearance increased tumor accumulation of murine CC49−Cy7. It has been reported previously that HuCC49ΔC_H2 has a modest decrease in tumor localization, as compared to the intact CC49.[49] Interestingly, Murine CC49−Cy7, HuCC49ΔC_H2−Cy7, and nonspecific IgG−Cy7 demonstrated a high level of distribution and long retention times in livers, which may be due to the chemical conjugation of the antibodies to the Cy7. The accumulation of murine CC49−Cy7 and HuCC49ΔC_H2−Cy7 conjugates in the liver was also similar to that reported in previous studies. For instance, the accumulation in the liver was also observed for chelated and radioisotope-labeled CC49[50] and single-chain Fv of CC49.[51] Mohsin et al.[50] suggested that the high accumulation in the liver was likely due to the metabolism of the chelated antibody in the liver. Clearance and

(48) Milenic, D. E.; Garmestani, K.; Chappell, L. L.; Dadachova, E.; Yordanov, A.; Ma, D. S.; Schlom, J.; Brechbiel, M. W. In vivo comparison of macrocyclic and acyclic ligands for radiolabeling of monoclonal antibodies with Lu-177 for radioimmunotherapeutic applications. *Nucl. Med. Biol.* **2002**, *29* (4), 431–442.

(49) Rogers, B. E.; Roberson, P. L.; Shen, S.; Khazaeli, M. B.; Carpenter, M.; Yokoyama, S.; Brechbiel, M. W.; LoBuglio, A. F.; Buchsbaum, D. J. Intraperitoneal radioimmunotherapy with a humanized anti-TAG-72 (CC49) antibody with a deleted CH2 region. *Cancer Biother. Radiopharm.* **2005**, *20* (5), 502–513.

metabolism of IgG antibody occur predominantly through the reticuloendothelial system (RES), primarily in the liver and spleen which contain the Kupffer cells. Furthermore, antibodies are bound and internalized by asialoglycoprotein receptors in the liver cells, increasing the retention of CC49 in the liver.[50] A long retention time for the antibodies in the liver and spleen was therefore expected.

Our dynamic imaging data also shows that pretreatment with excessive murine CC49 antibody could reduce the accumulation and retention times of murine CC49−Cy7 and HuCC49ΔC_H2−Cy7 conjugates in tumors (Figure 4). The results were confirmed by quantification of fluorescent signals in dissected tumor tissues (Figures 5A and 6A). In contrast, the accumulation of murine CC49−Cy7 and HuCC49ΔC_H2−Cy7 conjugates in the liver did not show significant change when the mice were pretreated with excessive CC49. This data suggests that murine CC49−Cy7 and HuCC49ΔC_H2−Cy7 specifically target the TAG-72 antigen in xenograft tumor tissues with nonspecific accumulation in the liver. Consistent with our finding, fluorescence intensities in the tumors were also observed to decrease when the xenograft nude mice were pretreated with overdose trastuzumab or C225 antibody to block HER2[52] or EGFr.[31] However, it was also reported that antibody blockage with cetuximab did not decrease fluorescence intensity in xenograft tumors on SCID mice.[38,39] The inconsistency may be caused by the different antibodies, tumor cells, animal models, and dosages of unlabeled antibody.

To optimize the efficacy of tumor detection, it is important to determine the point in time at which the maximum tumor to normal tissue ratio for the antibody is obtained. Mohsin et al. reported that the maximum tumor to blood ratios for ^{149}Pm-, ^{166}Ho-, and ^{177}Lu-MeO-DOTA-CC49 conjugates were obtained between 96−168 h postinjection.[50] Our dynamic imaging data (Figures 4A and 4B) also show that fluorescent intensity in the tumor reaches a high level at 120 h after injection of the murine CC49−Cy7, while the fluorescence intensity in the liver decreases to a low level at 96 h postinjection. Two additional groups of mice injected with the murine CC49−Cy7 conjugate were sacrificed at 2 and 96 h postinjection for fresh tissue imaging. The concentration of the murine CC49−Cy7 in the heart is regarded to be equal to the concentration of murine CC49−Cy7 in the blood. The tumor to heart ratio for murine CC49−Cy7 at 96 h postinjection was 15.5, which is comparable to previously reported data (34, 40). Chinn et al.[53] reported the tumor to blood ratio for ^{111}In-CC49 at 24 h postinjection to be 3.7 and Slavin-Chiorini et al.[47] reported the tumor to blood ratios for the iodine-CC49 at 24, 48, and 72 h postinjection to be 2.4, 3.0, and 7.4, respectively. The high tumor to heart ratio for the murine CC49−Cy7 obtained at 96 h postinjection suggests that 4 day after injection of the murine CC49−Cy7 is the optimal time for tumor detection and imaging using fluorescence.

Dynamic imaging showed that the concentration of the HuCC49ΔC_H2−Cy7 conjugate in the tumor decreased rapidly (Figure 4C). Therefore, we performed tumor imaging within 24 h postinjection of the HuCC49ΔC_H2−Cy7. The plasma clearance $t_{1/2}$ of the HuCC49ΔC_H2 in the LS-174T tumor-bearing athymic mice has been reported previously to range from 2.7 to 5.3 h,[48,49] suggesting that more than 90% of the HuCC49ΔC_H2 has been cleared from blood circulation at 18 h postinjection. Two additional groups of HuCC49ΔC_H2−Cy7 mice were sacrificed at 2 and 18 h postinjection for fresh tissue imaging. The tumor to heart ratio for the HuCC49ΔC_H2−Cy7 conjugate was determined to be 12.0. Our data are also consistent with previous findings which reported that ^{177}Lu-HuCC49ΔC_H2 and ^{111}In-HuCC49ΔC_H2 demonstrated tumor-to-blood ratios of 12.3 and 16.0 in LS174T xenograft mice at 24 h postinjection, respectively.[48,53]

Both murine CC49−Cy7 and HuCC49ΔC_H2−Cy7 conjugates accumulated to some extent in the spleen, kidneys, and lungs. However, the clearance of the antibodies from these tissues was faster compared to clearance from the tumor, suggesting that localization of murine CC49−Cy7 and HuCC49ΔC_H2−Cy7 conjugates in the spleen, kidneys, and lungs was not likely due to specific antigen−antibody interaction, as reported in a previous study.[51] The fluorescence observed from the kidneys was probably due to accumulation of metabolites of the antibody−Cy7 conjugates and nonspecific binding between the metabolites and brush border of the renal proximal tubule.[50]

In summary, we conjugated murine CC49 monoclonal antibody and HuCC49ΔC_H2 monoclonal antibody with a near-infrared (NIR) fluorophore Cy7 and tested the feasibility of the CC49−Cy7 and HuCC49ΔC_H2−Cy7 conjugates for NIR fluorescence imaging of tumors in a preclinical xenograft animal model. The results showed that antibody−Cy7 was indeed localized in tumor tissues. Murine CC49 antibody achieved a tumor/blood ratio of 15 at 96 h postinjection. In comparison, HuCC49ΔC_H2 was cleared much faster than murine CC49 in xenograft mice, and HuCC49ΔC_H2 antibody

(50) Mohsin, H.; Jia, F.; Sivaguru, G.; Hudson, M. J.; Shelton, T. D.; Hoffman, T. J.; Cutler, C. S.; Ketring, A. R.; Athey, P. S.; Simon, J.; Frank, R. K.; Jurisson, S. S.; Lewis, M. R. Radiolanthanide-labeled monoclonal antibody CC49 for radioimmunotherapy of cancer: Biological comparison of DOTA conjugates and Pm-149, Ho-166, and Lu-177. *Bioconjugate Chem.* **2006**, *17* (2), 485–492.

(51) Yokota, T.; Milenic, D. E.; Whitlow, M.; Wood, J. F.; Hubert, S. L.; Schlom, J. Microautoradiographic analysis of the normal organ distribution of radioiodinated single-chain Fv and other immunoglobulin forms. *Cancer Res.* **1993**, *53* (16), 3776–3783.

(52) Sampath, L.; Kwon, S.; Ke, S.; Wang, W.; Schiff, R.; Mawad, M. E.; Sevick-Muraca, E. M. Dual-labeled trastuzumab-based imaging agent for the detection of human epidermal growth factor receptor 2 overexpression in breast cancer. *J. Nucl. Med.* **2007**, *48* (9), 1501–1510.

(53) Chinn, P. C.; Morena, R. A.; Santoro, D. A.; Kazules, T.; Kashmiri, S. V. S.; Schlom, J.; Hanna, N.; Braslawsky, G. Pharmacokinetics and ibmor localization of In-111-labeled HuCC49 Delta C(H)2 in BALB/c mice and athymic murine colon carcinoma xenograft. *Cancer Biother. Radiopharm.* **2006**, *21* (2), 106–116.

achieved a tumor/blood ratio of 12 at 18 h postinjection. In contrast, Cy7 and nonspecific IgG−Cy7 had short retention times in the tumors. Additionally, for the mice pretreated with excessive murine CC49, the retention time of the murine CC49−Cy7 in the tumor was reduced from 288 to 240 h and the retention time of the HuCC49ΔC_H2−Cy7 was reduced from 96 to 48 h. These data suggest that both murine CC49−Cy7 and HuCC49ΔC_H2−Cy7 conjugates targeted TAG-72, and the excessive murine CC49 blocked the TAG-72 on the tumor. In conclusion, the Cy7 labeled murine CC49 and HuCC49ΔC_H2 demonstrate tumor-targeting capabilities in colorectal cancer xenograft mice and provide an alternative modality for tumor imaging.

Acknowledgment. We thank Dr. Jeffrey Schlom (Laboratory of Tumor Immunology and Biology, National Cancer Institute, National Institutes of Health, Bethesda, Maryland 20892) for his generous support of anti-Tag-72 antibodies and valuable suggestions for this study. This work was partially supported by Grant RO1 CA120023 to D.S. from National Cancer Institute (NCI).

MP9000052